



# Kinetics of crack-sealing, intergranular pressure solution, and compaction around active faults

François Renard<sup>a,\*</sup>, Jean-Pierre Gratier<sup>b</sup>, Bjørn Jamtveit<sup>a</sup>

<sup>a</sup>*Fluid–Rock Interactions Group, University of Oslo, Departments of Geology and Physics, P.O. Box 1047 Blindern, 0316 Oslo, Norway*

<sup>b</sup>*LGIT, CNRS-Observatoire, Université Joseph Fourier BP 53, 38041 Grenoble cedex, France*

Received 17 January 2000; accepted 18 May 2000

## Abstract

Geological evidence indicates that fluids play a key role during the seismic cycle. After an earthquake, fractures are open in the fault and in the surrounding rocks. With time, during the interseismic period, the permeability of the fault and the country rocks tends to decrease by gouge compaction and fracture healing and sealing. Dissolution along stylolite seams provides the matter that fills the fractures, whereas intergranular pressure solution is responsible for gouge compaction. If these processes are fast enough during the seismic cycle, they can modify the creep properties of the fault. Based on field observations and experimental data, we model the porosity decrease by pressure solution processes around an active fault after an earthquake. We arrive at plausible rates of fracture sealing that are comparable to the recurrence time for earthquakes. We also study the sensitivity of these rates to various parameters such as grain size, fracture spacing, and the coefficient of diffusion along grain boundaries and stylolites. © 2000 Elsevier Science Ltd. All rights reserved.

## 1. Roles of fluids in faults

The interest in slip instability has increased considerably since Brace and Byerlee (1966) proposed that it might be related to earthquake rupture (see Scholz, 1990 for an historical review). As geologic evidence is gathered on the involvement of fluids in faults, a growing number of researches have started to study the effects of fluid pressure on fault mechanics (Lachenbruch, 1980; Sleep and Blanpied, 1994; Chester, 1995; Hickman et al., 1995; Segall and Rice, 1995; Matthai and Fisher, 1996; Lockner and Byerlee, 1995; Fournier, 1996; Miller et al., 1996; Yamashita, 1997; Henderson and Maillot, 1997). Byerlee (1990) and Rice (1992) suggested that the relative weakness of some faults could be due to high intra-fault fluid pressure. Overpressuring could be generated and maintained by the flow of deep fluids into the ductile roots of a fault

zone (Rice, 1992). On the other hand, high overpressure can be sustained by conjecturing efficiently sealed compartments and gouge compaction (Byerlee, 1990; Sleep and Blanpied, 1994). In both cases, earthquakes are assumed to take place when the fluid pressure is close to lithostatic values. Because of dilatancy and fault connectivity increase, earthquakes are assumed to reduce the fluid pressure to hydrostatic levels. As a consequence, the fluid pressure varies between two end-member values during the seismic cycle.

In a model of fluid flow in partially sealed fault zones, Sleep and Blanpied (1994) assumed a purely viscous rock behavior. The pressure equation was based on the conservation of fluid phase and included both an increase in pressure due to compaction and a decrease in pressure due to escape of fluid. In the case of a single fault system, they showed that the increased fluid pressure allows frictional failure and earthquakes at shear traction far below that required when fluid pressure is hydrostatic. Segall and Rice (1995) have developed a model of unstable slip by modifying the rate and state dependent friction model to include fluid

\* Corresponding author.

*E-mail address:* francois@geologi.uio.no (F.Fran. Renard).

pressure and porosity. This model is based on porosity changes deduced from gouge experiments (Marone et al., 1990) with overcompacted rocks where one observes an increase of porosity with shear strain if the normal stress is kept constant. This is called the dilatancy hardening effect (Rice, 1975; Rudnicki and Chen, 1988). Henderson and Maillot (1997) used an empirical exponential function to describe the reduction of porosity due to compaction. They assumed that in the case of rupture, porosity could increase up to 10%. Miller et al. (1996) presented a discrete instability model assuming that the normal stress compacts the fault zone and reduces the porosity, resulting in high fluid pressured compartments and a local weakening of the fault.

As this short literature survey reveals, porosity and permeability are assumed to vary during the seismic cycle, but the porosity changing mechanisms and the precise time scales of these mechanisms are still controversial.

In addition to these models, observations of exhumed faults provide many evidence of extensive fluid–rock interactions (Evans and Chester, 1995), in particular, pressure solution processes can be demonstrated by indented grains and stylolites (Gratier and Gamond, 1990; Janssen et al., 1997). Some of the most significant observations may be summarized as follows. Fluid inclusion networks in the vein minerals demonstrate the presence of fluids during the crack sealing and reflect self-healing processes within the sealing deposit. However, the veins related to active faults are always sealed by external input of material (Gratier et al., 1994; Evans and Chester, 1995). The source of this vein material is mostly nearby solution cleavage and stylolites in the country rocks. This can be demonstrated both by geometric arguments (veins interrupted

against solution surface) and by chemical arguments (same mineral dissolved in solution cleavage and precipitated in veins—see Fig. 1) (Gratier et al., 1994). Therefore pressure solution associated with deposition in veins is the main mechanism of crack sealing around active faults and in the gouge.

The nature and the origin of fluids and sealing minerals in fault systems can be estimated from isotope studies. In the San Andreas system, California, the isotope composition of samples from gouges and vein-filling minerals have been compared with that of the host rocks by Pili et al. (1998). The results indicate that fault zones formed at depths between 2 and 5 km appear to have been infiltrated during deformation by fluids of deep origin dominated by crustal water. Mineral deposit in gouges and veins may thus be considered as representing a mixture of species dissolved in the external fluid and species from the dissolving country rocks.

This is compatible with observations indicating that from time to time, probably after an earthquake occurrence, gouge and veins are hydraulically connected. Then, during the interseismic period, vein sealing occurs by input of material removed by pressure solution processes in the nearby country rocks. This type of crack seal model is also compatible with the results of Fisher et al. (1995) who found that there is no evidence for long distance transport of silica within the Kodiak convergent prism in Alaska. However, there is geochemical evidence of local migration of silica from the rock matrix to veins with an approximate balance between the silica dissolved from the rock matrix and the amount of quartz precipitated in veins (Fisher and Brantley, 1992).

From the observed natural structures, the following sequence of crack-sealing processes is expected to occur in active fault zones during interseismic periods (Gratier et al., 1994). Initially, rapid slip driving an earthquake will cause an increase of the overall permeability and reduce the fluid pressure to levels approaching hydrostatic values within the fault zone. The first stage of fluid/rock interactions occurs on the free faces produced during the earthquake and is characterized by fast kinetics. Self-healing of fractured minerals and growth of metamorphic minerals are relevant to this stage. However, none of these processes significantly contribute to the sealing of the open cracks (Gratier et al., 1994). The second stage is pressure solution creep, associated with the indentation of grains and the dissolution along stylolites. It is found to be much more efficient and can be thought as a mechanism that relaxes the stresses in and around the fault. It also decreases the effective stress imposed on the matrix by compaction of the gouge. According to experiments, the time scales of such crack sealing, controlled by the kinetics of pressure solution and associ-

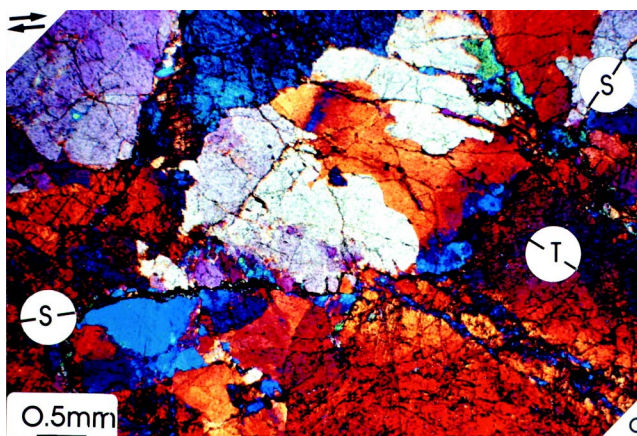


Fig. 1. Thin section of crack sealing of veins in a granite rock from the San Gabriel Fault, California. Dissolution occurs along stylolites (S) and solutes precipitate locally in veins open in tension (T). In this case, the cracks are thin (5–10  $\mu\text{m}$ ) and the mean distance between stylolites is 100–200  $\mu\text{m}$ . Adapted from Gratier et al. (1994).

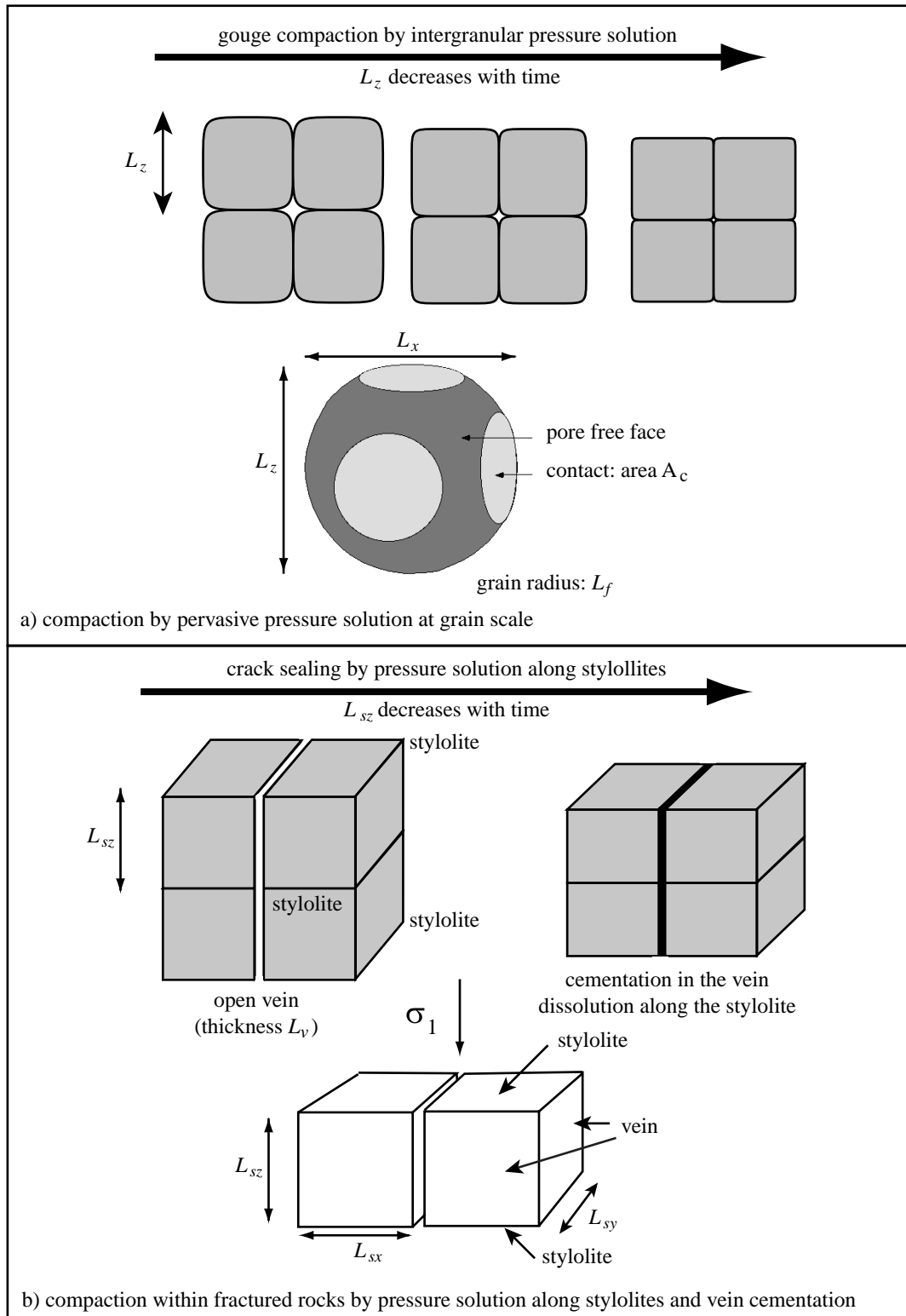


Fig. 2. Textural model for compaction by pressure solution during the interseismic period. Compaction occurs through two mechanisms: pervasive pressure solution at the grain scale (gouge), and vein cementation associated with dissolution along stylolites (country rock around an active fault). (a) Model of truncated sphere for intergranular pressure solution. (b) Model of vein cementation and dissolution along stylolites. The different lengths are used in Eqs. (2)–(10). Both mechanisms are responsible of a creep-like deformation of the rock, with different characteristic time scales.

ated with deposition processes, are on the order of several tens of years to several million years and are strongly dependent on temperature and the rock texture (Rutter, 1976; Hickman and Evans, 1991; Gratier, 1993). Modeling such an evolution requires knowledge of the geometry of the transport pathways controlling the rate of mass transfer. In this paper, we consider two schemes of porosity reduction

1. Compaction modeling of the gouges by pervasive pressure solution at grain contacts associated with precipitation of the dissolved matter in the pore space (Fig. 2a). This mechanism leads to grains indentation and an overall porosity decrease (Renard et al., 1999).
2. Crack-seal and creep around the faults by mass transfer between dissolution surfaces (i.e. stylolites), oriented perpendicularly to the maximum compressive stress direction and associated with precipitation on surfaces in contact with free fluid in open cracks (Fig. 2b).

We attempt to quantify the kinetics of these two mechanisms by a conceptually simple reaction and local transport model. The effects of various par-

ameters such as stress, rock texture, diffusion rates and temperature are also studied.

## 2. A model for pressure solution and crack sealing

### 2.1. The driving force for pressure solution

Stress has a significant effect on the chemical potential of a solid. The effect is to increase its molar free energy compared to that at zero-stress. Though the Gibbs-type free energy cannot be defined for nonhydrostatically stressed solids (Shimizu, 1995), dissolution/precipitation of solids is fully described by the surface chemical potential  $\mu$  (Gibbs, 1877). If tangential stress on the grain surface is zero, the chemical potential difference over a grain surface can be written

$$\Delta\mu = \Delta f + \bar{V}_s \Delta P_n \quad (1)$$

where  $\mu$  is the chemical potential of the dissolved component,  $P_n$  is the normal pressure on the solid,  $f$  represents the molar Helmholtz free energy,  $\bar{V}_s$  is the molar volume of the solid (see Table 1 for notations

Table 1  
Symbols used in Eqs. (1)–(19) and Fig. 2

$F$	Free energy (J mole <sup>-1</sup> )
$\mu$	Chemical potential (J mole <sup>-1</sup> )
$\mu_0$	Chemical potential in a reference state
$K_{\text{eq}}$	Equilibrium constant of a chemical reaction
$K_0$	Equilibrium constant in a reference state
$c_{\text{H}_4\text{SiO}_4}$	Concentration of silica in solution (mole m <sup>-3</sup> )
$a_{\text{H}_4\text{SiO}_4}$	Activity of silica in solution
$\gamma_{\text{H}_4\text{SiO}_4}$	Activity coefficient of silica in solution
$c_c$	Concentration within the grain contact (mole m <sup>-3</sup> )
$c_s$	Concentration in the stylolite (mole m <sup>-3</sup> )
$c_p$	Concentration in the pore fluid (mole m <sup>-3</sup> )
$c_v$	Concentration in vein
$K_p$	Kinetics constant for precipitation of the pore surface (mole m <sup>-2</sup> s <sup>-1</sup> )
$\Delta$	Thickness of the water film trapped inside the grain contact (m)
$D_c$	Coefficient of diffusion along the grain contact (m <sup>2</sup> s <sup>-1</sup> )
$\bar{V}_s$	Molar volume of a mineral (m <sup>3</sup> mole <sup>-1</sup> )
$T$	Temperature (K)
$P_i$	Normal stress in direction $i$ ( $x$ , $y$ or $z$ ) (bar)
$P_s$	Normal stress to a stylolite (bar)
$P_p$	Pore pressure (bar)
$\phi$	Gouge porosity
$\phi_{\text{frac}}$	Fracture porosity
$L_x, L_y, L_z$	Grain parameters to describe the truncated sphere geometry of Fig. 2(a) (m)
$L_v$	Thickness of the open vein (m)
$L_{sx}, L_{sz}$	Distance between stylolites in the $x$ and $y$ directions (m)
$L_f$	Grain radius (m)
$A_c$	Surface area of contact between two grains (m <sup>2</sup> )
$l_c$	Radius of a grain contact ( $\pi l_c^2 = A_c$ ) (m)
$G_c$	Velocity of dissolution at grain contacts (m s <sup>-1</sup> )
$G_p$	Velocity of precipitation on the pore surface (m s <sup>-1</sup> )
$G_s$	Velocity of dissolution along a stylolite (m s <sup>-1</sup> )
$G_v$	Velocity of precipitation in the open vein (m s <sup>-1</sup> )

and units). Relationship Eq. (1) characterizes the chemical potential at the solid at each point on the surface of the solid and varies over the grain surface between contact areas and pore surface. The driving force for material transfer along a grain surface is the difference in chemical potential between two parts of the same crystal surface. The term  $\Delta f$  contains contributions due to elastic energy, dislocation energy and surface energy. At the conditions prevailing in the earth's crust, these different contributions are one to two orders of magnitude less than the contribution of the normal stress, and this is often neglected (Paterson, 1973).

2.2. A textural and stress model for intergranular pressure solution

The non-linear dynamics of grain compaction in the gouge arise from the fact that during deformation intergranular contact areas grow and grains indent each other. To account for such geometric evolution, the rock is modeled as a cubic array of grains (Dewers and Ortoleva, 1990; Renard et al., 1999) and assumed to be monomineralic. The grains have a truncated spherical geometry (Fig. 2a), which is characterized by four geometrical lengths:  $L_f$ , the grain radius, and  $L_x$ ,  $L_y$ , and  $L_z$ , the lengths of the truncations in the three directions of space. Intergranular fluids can be considered as fluid films (Weyl, 1959; Rutter, 1976) or as a connected network of fluid inclusions, forming an 'island and channel' pattern (Raj and Chyung, 1981; Spiers et al., 1990). In our simulations we will simply describe the grain boundary as a fluid film. This assumption should only modify the transport properties of the grain contacts, the diffusion being faster in the presence of an 'island and channels' structure.

Compaction at a grain scale can be divided into three successive steps (Raj, 1982; Renard et al., 1997). Dissolution occurs at grain contacts due to a local concentration of stress. Then solutes diffuse along the grain/grain interface where a fluid film is trapped (Renard and Ortoleva, 1997). When arriving in the pore, the solutes precipitate on the surface of the grain in contact with the pore space. The whole process is responsible for a non-linear porosity reduction with time.

The complex dynamics of pressure solution comes from a non-linear feedback between stress and rock texture. Following the analysis by Dewers and Ortoleva (1990) one can write a force balance relationship between the vertical stress  $P_z$  (equivalent to a lithostatic stress, for example the effect of overburden), the normal stress on a grain contact  $P_c$ , and the pore pressure  $P_p$ :

$$-L_x L_y (P_z - P_p) P_z = A_c P_c + (L_x L_y - A_c) P_p \quad (2)$$

where  $A_c$  is the surface area of the contact and  $L_x$ ,  $L_y$  are the truncations of the spherical grains in the  $x$  and  $y$  directions, as shown in Fig. 2(a). As  $A_c$  increases with time, the stress normal to the contact decreases allowing a coupling between grain geometry and stress. For simplicity, we focus on the vertically directed grain contacts (normal to the  $z$ -axis). Results are identical for the horizontally directed contacts (normal to  $x$  and  $y$  contacts) because one considers an isotropic loading of the system.

The velocities  $G_c$  and  $G_p$  ( $m\ s^{-1}$ ) describe the geometric evolution of the  $z$ -contact length variables.  $G_c$  is representative of the time evolution of the moving grain interface due to dissolution at contact and represents the rate at which  $L_z$  decreases with time.  $G_p$  takes in account the evolution of the grain radius and characterizes the thickness of overgrowth on the pore surface (Renard et al., 1999). Given these rates, the textural evolution of the grains follows:

$$\frac{dL_z}{dt} = G_c(c_c, P_c, P_z) \text{ and } \frac{dL_f}{dt} = G_p(c_p, P_p, P_z) \quad (3)$$

where  $L_f$  is the grain radius,  $L_z$  is the length of the truncation of the spherical grain,  $c_c$  and  $c_p$  are the concentrations inside the contact and in the pore respectively;  $P_c$  is the normal stress in the contact,  $P_p$  is the pore pressure and  $P_z$  is the lithostatic vertical pressure. The rates  $G$  are defined positive when dissolution occurs on the surface and negative for precipitation. In the model  $c_c$  is related to  $c_p$  by a steady state assumption (Dewers and Ortoleva, 1990). Fick's Law gives

$$\frac{2\pi l_c \Delta D_c (c_c - c_p)}{l_c} = -\frac{A_c}{\bar{V}_s} G_c \quad (4)$$

where  $\bar{V}_s$  is the molar volume of the dissolving solid,  $D_c$  is the diffusion coefficient along the grain boundaries,  $\Delta$  is the thickness of the water film trapped in the grain interface,  $l_c$  is the radius of the circular grain contact, and  $A_c$  its surface area. We must also take into account the conservation of volume in a system closed at a grain scale

$$6A_c G_c + A_p G_p = 0. \quad (5)$$

The factor 6 in Eq. (5) represents the six contacts that each grain has with its neighbors. The rate  $G_p$  corresponds to the precipitation on the pore surface, which is equal to

$$G_p = k_p \bar{V}_s \left( 1 - \frac{c_p}{K_{eq}} \right) \quad (6)$$

where  $k_p$  is the kinetics constant for mineral precipitation and  $K_{eq}$  the equilibrium constant for the reaction of dissolution/precipitation. The ratio in Eq. (6) represents the degree of super-saturation. This model

of dissolution at grain contacts and precipitation on the free face allows an overall compaction of the rock.

### 2.3. A textural and stress model for stylolites and veins

Dissolution occurs along the stylolite planes and matter is transported to the open veins oriented perpendicularly to the stylolites. The mean distance between stylolites  $L_{sz}$  decreases with time due to dissolution. During the same time, the open veins close because of precipitation and  $L_{sx}$  and  $L_{sy}$  are increasing whereas the open space in veins  $L_v$  is decreasing (Fig. 2b). The process stops when the original open fracture becomes filled and attains zero percent porosity. The fracture porosity  $\phi_{\text{frac}}$  of the system is equal to

$$\phi_{\text{frac}} = \frac{L_v(L_{sx} + L_{sy})}{(L_{sx} + L_v)(L_{sy} + L_v)} \quad (7)$$

As in the case of intergranular pressure solution, the stress normal to the stylolite surface decreases with time as precipitation occurs in the veins. One can also write a relationship similar to Eq. (2) between the macroscopic stress perpendicular to the stylolite  $P_z$ , (here similar to a lithostatic stress), the normal stress on a stylolite surface  $P_s$ , and the pore pressure  $P_p$

$$(L_{sx} + L_v)^2 P_z = L_{sx}^2 P_s + 2L_{sx} L_v P_p \quad (8)$$

where it is assumed that  $L_{sx} = L_{sy}$ .

Deformation occurs by dissolution of matter in stylolite planes perpendicular to the main stress  $\sigma_1$  and solutes precipitate in open veins perpendicular to  $\sigma_2 = \sigma_3$ . Thus it follows that

$$\frac{dL_{sz}}{dt} = G_s(c_s, P_s) \quad (9)$$

$$\text{and } \frac{dL_{sx}}{dt} = \frac{dL_{sy}}{dt} = -\frac{dL_v}{dt} = G_v(c_v, P_p)$$

where  $L_{sx}$  and  $L_{sy}$  are assumed to be equal. The rate  $G_s$  describes the decrease of thickness of the interstylolitic region due to dissolution along the stylolite surface;  $c_s$  is the concentration of dissolved matter in the stylolite and  $P_s$  the stress normal to the stylolite.  $G_v$  is the rate of precipitation inside the vein,  $c_v$  is the concentration of solutes in the open vein and  $P_p$  the fluid pressure inside the vein, assumed to be equal to the pore pressure (equal to  $\sigma_2$  and  $\sigma_3$ ).

In the model  $c_s$  is related to  $c_v$  by a Fick's law describing diffusion from the stylolite to the veins

$$\frac{4L_{sy}\Delta_s D_s(c_s - c_v)}{L_{sy}} = -\frac{L_{sx}^2}{\bar{V}_s} G_s \quad (10)$$

where  $\bar{V}_s$  is the molar volume of the dissolving solid,

$\Delta_s$  is the thickness of the stylolite, and  $D_s$  is the diffusion coefficient of the dissolving solute along the stylolite. The value of the diffusion coefficient along a stylolite is not well defined, but for a given temperature, it should range between that at a single grain contact (as measured in pressure solution experiments) and that in a very fine-grained rock such as an ultramylonite or a quartz aggregate (Farver and Yund, 1995, 1999). For example, at 200°C, a typical values for the diffusion coefficient in a mylonite, estimated after Farver and Yund (1999), is  $9.8 \times 10^{-15} \text{ m}^2 \text{ s}^{-1}$ , with an activation energy of  $30 \pm 6 \text{ kJ mole}^{-1}$ . This value can vary within an order of magnitude, depending on whether diffusion is parallel or perpendicular to the mylonite schistosity. Pressure solution experiments indicate that the product of water film thickness and coefficient of diffusion is around  $10^{-19} - 10^{-20} \text{ m}^3 \text{ s}^{-1}$  at 350°C (Rutter, 1976; Gratier and Guiguet, 1986) with a smaller activation energy. For a flat grain interface of 1 nm, this means that the coefficient of diffusion at the grain contact would be  $10^4 - 10^5$  greater than for the case of an ultramylonite.

As for the model of pressure solution at grain scale, we must take into account the conservation of volume in a closed system. All the matter dissolved inside the stylolite precipitates in the veins.

$$2L_{sx}^2 G_s + 4L_{sx} L_{sz} G_v = 0 \quad (11)$$

The rate  $G_v$ , representing precipitation on the vein surface, is defined as in Eq. (6), except that the concentration is that in the open vein

$$G_v = k_p \bar{V}_s \left( 1 - \frac{c_v}{K_{\text{eq}}} \right) \quad (12)$$

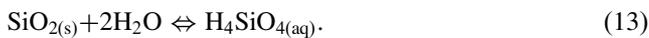
### 3. Modeling the compaction within and around a fault

The gouge is considered to be an aggregate of either pure quartz or pure calcite with a grain size of 10  $\mu\text{m}$  in the gouge. Just after an earthquake, the porosity of this rock is high and estimated to be around 10% from evaluation of the mean ratio between sealed cracks and host rocks. This value is also taken as an initial condition for gouge compaction to compare the two processes. The initial mean distance between veins and stylolites in the country rock is taken from geological observations ( $L_{sx} = L_{sy} = L_{sz} = 100 \mu\text{m}$ ) (Fig. 1; Gratier et al., 1994; Gudmundsson, 1999). Just after an earthquake, the fractures are considered to be open, with a thickness  $L_v = 6 \mu\text{m}$  (Gratier et al., 1994). Given these conditions, the initial fracture porosity of the system is close to 10%. We apply our model to estimate pressure solution rates in pure limestone and quartz rocks. These initial conditions will be varied

later to study the effect of the distance of transport between sites of dissolution and sites of precipitation.

The transport properties of the grain interface and the stylolites are taken from experiments on pressure solution (Rutter, 1976; Hickman and Evans, 1991; Gratier and Guiguet, 1986; Gratier, 1993) which give the product coefficient of diffusion times water film thickness in the range  $10^{19}$ – $10^{21}$  m<sup>3</sup> s<sup>-1</sup> at 250 to 350°C. A small activation energy of 15 kJ/mole is taken to estimate this product at lower temperatures. The thickness of the flat grain interfaces is assumed to decrease exponentially as the effective stress increases (Renard and Ortoleva, 1997).

We consider now two simple end-member cases. The rock is monomineralic and can be either pure quartz or pure calcium carbonate. The chemical reaction of dissolution or precipitation of quartz is taken to be



The equilibrium constant for this reaction  $K_{\text{eq}}$  is

$$K_{\text{eq}} = \frac{a_{\text{H}_4\text{SiO}_4}}{a_{\text{SiO}_2} a_{\text{H}_2\text{O}}} \quad (14)$$

where all the *a*s are the activity of the species in sol-

ution. At equilibrium, if we take the reference states of solid quartz and water to be pure stress-free states and we take the activities of quartz and water equal to 1. The equilibrium constant is related to silica solubility  $c_{\text{H}_4\text{SiO}_4}$  through

$$K_{\text{eq}} = \gamma_{\text{H}_4\text{SiO}_4} c_{\text{H}_4\text{SiO}_4} \quad (15)$$

where  $\gamma_{\text{H}_4\text{SiO}_4}$  is the activity coefficient, assumed to be equal to 1 in a dilute pressure free state and  $c_{\text{H}_4\text{SiO}_4}$  is the molarity of aqueous silica.  $K_{\text{eq}}$  under stress is related to the equilibrium constant  $K_0$  in stress-free state by

$$K_{\text{eq}} = K_0 \exp\left(\frac{\mu_{\text{qz}} - \mu_0}{RT}\right) \quad (16)$$

Using these relations one can estimate the solubility of quartz on the different sites of the model (grain contact, pore surface, stylolites, veins). Such solubility enters the model through the reaction of precipitation in the pore (Eqs. (6) and (12)). In Eq. (16),  $K_0$  is almost only dependent on temperature, the pressure dependence being included in the free-energy term. It is the equilibrium constant for a stress-, dislocation-, elastic- and surface energy-‘free’ state. We choose its value to be as following (Rimstidt and Barnes, 1980)

$$\log(K_0) = 1.881 - 0.002028 \times T - \frac{1560}{T} \quad (17)$$

The rate constant for dissolution/precipitation increases with temperature and varies with pH and ionic concentrations (Dove, 1994). Some authors have evaluated the kinetics of quartz dissolution through laboratory measurements (Dove, 1994) and found rates faster than in geological conditions (Oelkers et al., 1996). Walderhaug (1994) has derived precipitation rates in sandstones in the Norwegian shelf from fluid inclusion microthermometry and he has found a value much lower. Because of the large uncertainty about the kinetics of quartz dissolution-precipitation, we have chosen kinetics laws derived from data measured in laboratory (Dove, 1994), even if in geological conditions inhibitions processes could slow down the kinetics of dissolution-precipitation.

The reaction of calcite dissolution is taken to be



Plummer and Busenberg (1982) give the following relationship for the equilibrium constant of this reaction between 0 and 90°C

$$\log(K_{\text{eq}}) = -171.065 - 0.0077993T + 2839.319/T + 71.595 \log(T) \quad (19)$$

where  $T$  is the temperature in Kelvin. We have also

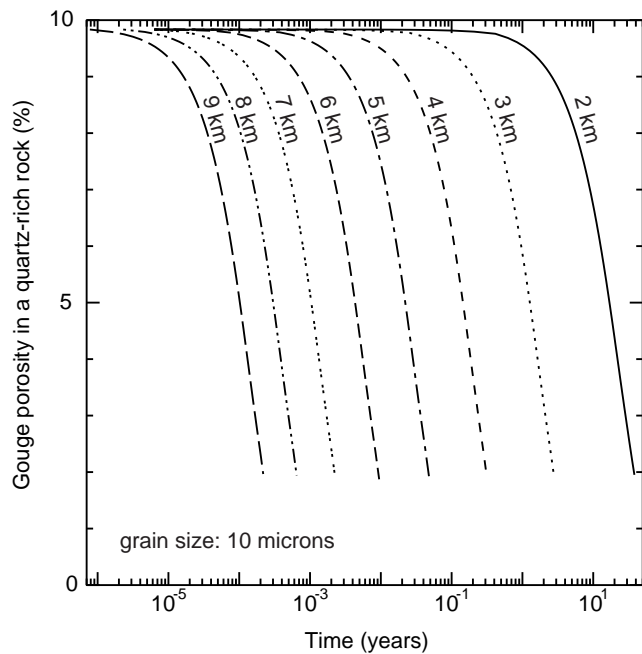


Fig. 3. Simulations of the compaction of a quartz gouge with fine grains (10 μm). The porosity decreases with time due to pervasive pressure solution. Initially, the porosity of the gouge is high (around 10%) and it decreases because of dissolution at grain contacts and precipitation in the pores (see Fig. 2a). The porosity–time curves are almost linear in this logarithmic–linear graph indicating an exponential decrease of porosity with time with characteristic times decreasing with depth. In these and the next simulations, the temperature gradient is 30°C/km and the lithostatic and hydrostatic pressure gradients are taken to be 22 MPa/km and 10 MPa/km, respectively.

used their model of  $\text{CO}_2\text{-H}_2\text{O}$  equilibrium to estimate the concentrations of  $\text{CO}_3^{2-}$ ,  $\text{HCO}_3^-$ , and  $\text{H}_2\text{CO}_3$ , as well as the activity of dissolved  $\text{CO}_2$  between 0 and  $90^\circ\text{C}$ . Above this temperature, the equilibrium constant for this reaction is estimated with the SUPCRT92 database (Johnson et al., 1992). The kinetics constant of calcite dissolution and precipitation was calculated from Plummer et al. (1978, 1979).

Compaction and stylolitization are modeled for different geological conditions corresponding to a vertical profile in the crust along a fault between 2 and 9 km depth. A temperature gradient of  $30^\circ\text{ km}^{-1}$  is taken. As stated in the introduction, the driving force for gouge compaction after an earthquake is assumed to be the difference between lithostatic and hydrostatic pressure. The hydrostatic pressure gradient is chosen to be  $10\text{ MPa km}^{-1}$  and the lithostatic pressure gradient is  $22\text{ MPa km}^{-1}$  (here assumed to correspond to  $\sigma_1$ ). We will consider only the case of a hydrostatic fluid pressure. Overpressure compartments may develop in the faults during the interseismic period, and this should modify the driving force for pressure solution deformation. However, overpressuring is a complex process which is dependent not only on the

evolution of the porosity of both the gouge and the country rocks, but also on the flux of fluid from depth (Rice, 1992). As we intend to compare the rate of change of porosity between two mechanisms (grain compaction, and stylolites–veins) we think it is interesting to use a comparable driving force. However it must be kept in mind that the evolution with time of both rates of change of porosity may be slower than estimated when overpressuring develops.

For stylolites and vein-sealing the driving force is the shear along the fault plane which induces a difference of normal stress between the stylolites and the veins. Few data are available on the evolution of such a difference of stress with depth; so we took an evolution similar to the driving force for the gouge, assuming a constant increase of the normal stress difference with depth ( $12\text{ MPa km}^{-1}$ ). Moreover it has been observed that in the upper crust the effective stress variation has a smaller influence on the rate of deformation, than the temperature variation (Oelkers et al., 1996; Walderhaug, 1994). In our simulations, the increase of temperature with depth induces a greater effect on the increase of the pressure solution rate than effective stress variations would.

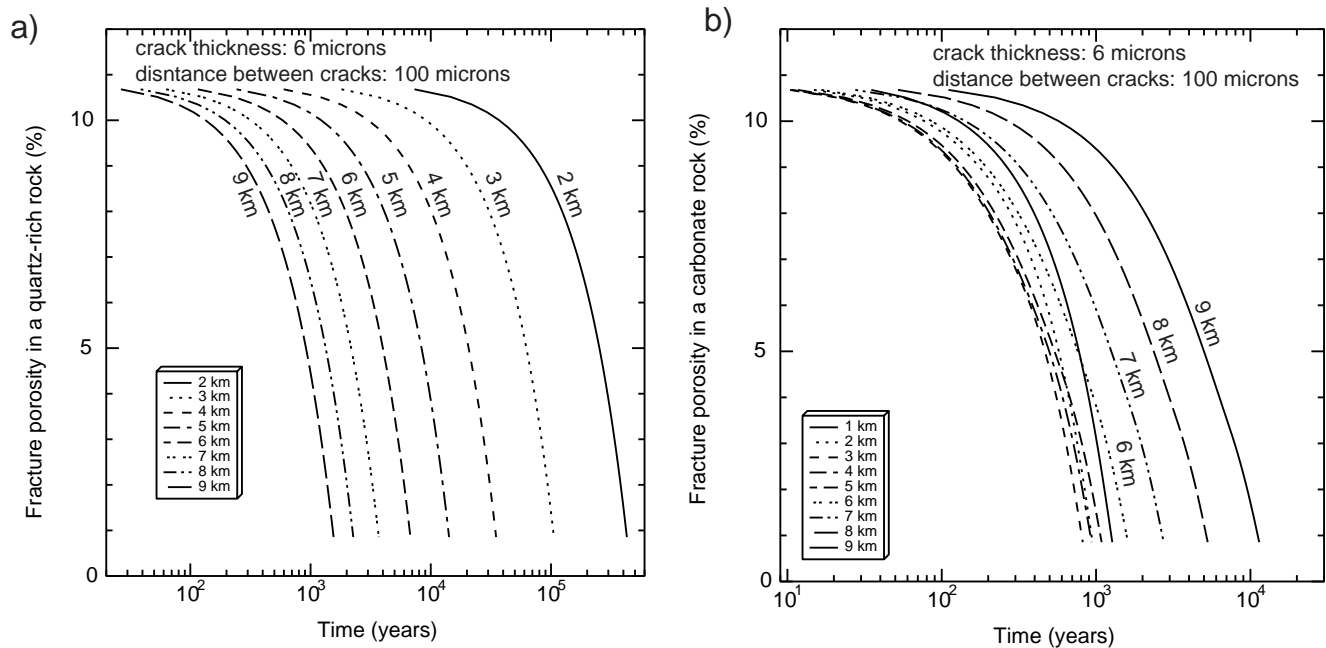


Fig. 4. (a) Pressure solution by stylolitization and precipitation in quartz veins as a function of time. The fracture porosity, initially arbitrarily fixed at around 10% just after an earthquake, decreases with time. The curves correspond to different depths between 2 and 9 km. (b) Pressure solution by stylolitization and precipitation in calcite veins as a function of time. As for quartz, the fracture porosity is arbitrarily fixed at around 10% just after an earthquake. The curves correspond to simulations at different depths between 1 and 9 km. Between 2 and 5 km, the rate of pressure solution does not change with depth. This is due to two antagonistic processes. On one hand, the solubility of calcium carbonate decreases with temperature and depth, lowering the pressure solution rate. On the other hand the increasing effective stress with depth promotes the rate of pressure solution. These two effects cancel with depth. Below 5 km, the solubility decrease is faster than the increase of driving force related to stress. Therefore the rate of pressure solution decreases. The characteristic times for deformation are greater for crack sealing than in the gouge (Fig. 3), mainly because of an increase of the distance of transport.

### 3.1. Quartz grain deformation in the gouge

During chemical compaction, dissolution occurs inside the grain contact and matter precipitates on the pore surface, hence  $L_f$  (measuring the thickness of overgrowth on the pore surface) increases (Fig. 2a). It is assumed that chemical compaction is isotropic, so grain truncation lengths  $L_x$ ,  $L_y$ , and  $L_z$  all decrease equally with deformation. The model is closed at the grain scale with respect to solid mass, thus the grain volume does not change with time. The grains evolve as truncated spheres with decreasing pore surface area and increasing nominal contact area (Fig. 2a). Simultaneously, porosity decreases with time (Fig. 3). Depending on depth, it takes from less than 1 day (at 9 km) to 50 y (at 2 km) to close the porosity in a quartz-rich gouge with very fine texture (grain size of 10  $\mu\text{m}$ ). In this case of very fine-grained rocks, pressure solution would be very fast and it would represent a relevant mechanism for post-seismic viscous relaxation in the gouge of an active fault at depth.

### 3.2. Stylolite–vein deformation in the fault

Due to quartz dissolution along stylolites and precipitation in the veins, the fracture porosity  $\phi_{\text{frac}}$  of the

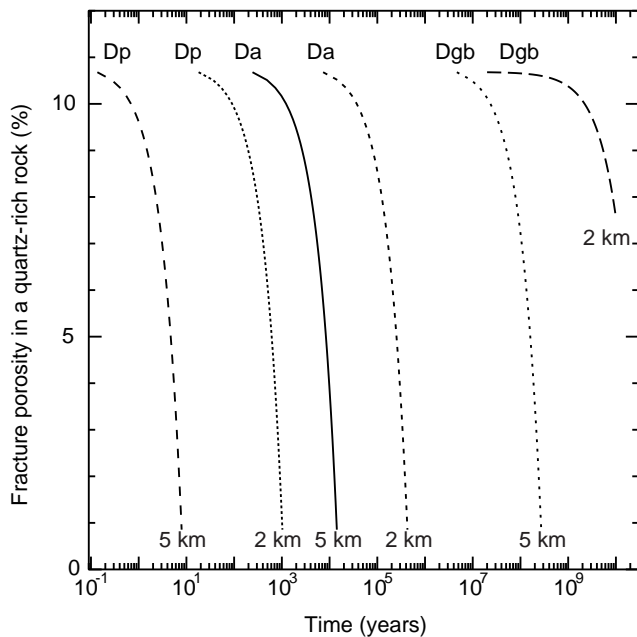


Fig. 5. Deformation rates for crack sealing in a quartz-rich rock. Initial conditions are the following: mean distance between stylolites ( $L_{sz}$ ): 100  $\mu\text{m}$ , crack aperture ( $L_v$ ): 6  $\mu\text{m}$ . The deformation rate decreases slowly with time as deformation occurs because the stress normal to stylolites decreases as cracks seal (Eq. (8)). The effect of depth on the rate of pressure solution is clearly seen, the main effect being the increase of temperature that modify the solubility of silica in water by several orders of magnitude (Eqs. (9) and (10)).

rock decreases with time (Fig. 4a). If this porosity is arbitrarily fixed at 10% after an earthquake, it decreases to 0% in 1000 y at 9 km depth, or 0.4 My at 2 km depth for a quartz-rich lithology. These fracture-healing rates are 3–4 orders of magnitude slower than for compaction of the gouge. They correspond to deformation rate increasing by two orders of magnitude from 2 to 9 km (Fig. 5).

In the case of calcite, the fracture porosity closes in about 1000 y (Fig. 4b) between 2 and 5 km and the compaction rate slows down below. It seems that the rate of pressure solution does not change much with depth in carbonate-rich rocks between 2 and 5 km. This is due to two opposite effects that cancel each other. On one hand, an increase of temperature with depth decreases calcite solubility and the rate of pressure solution. On the other hand, the effective stress increases with depth and promotes the driving force for pressure solution. Below 5 km, the rate of pressure solution decreases constantly because the solubility decrease is not compensated by the increase of effective stress.

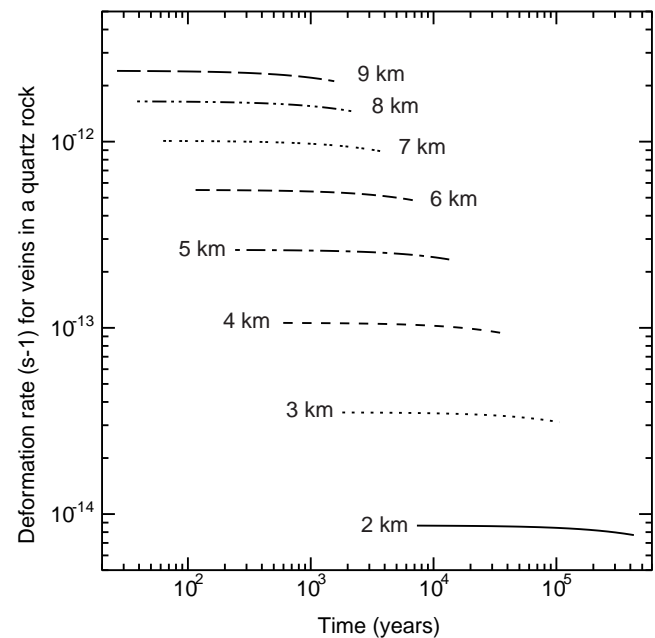


Fig. 6. Sensitivity of the rate of crack sealing to the value of the coefficient of diffusion along the stylolite for simulations corresponding to a quartz-rich rock at 2 and 5 km depth.  $D_{gb}$  is the coefficient of diffusion as estimated by Farver and Yund (1999) for a highly stressed mylonite (activation energy 30  $\text{kJ mole}^{-1}$ ),  $D_a$  is the coefficient of diffusion for a 2-nm-thick water film as estimated from pressure solution experiments (activation energy 15  $\text{kJ mole}^{-1}$ ) (Rutter, 1976; Hickman and Evans, 1991; Gratier and Guiguet, 1986; Gratier, 1993) and  $D_p$  is the coefficient of diffusion in bulk water (activation energy 15  $\text{kJ mole}^{-1}$ ) (Applin, 1987). The time associated with pressure solution is strongly dependent on the diffusion rate at grain boundaries.

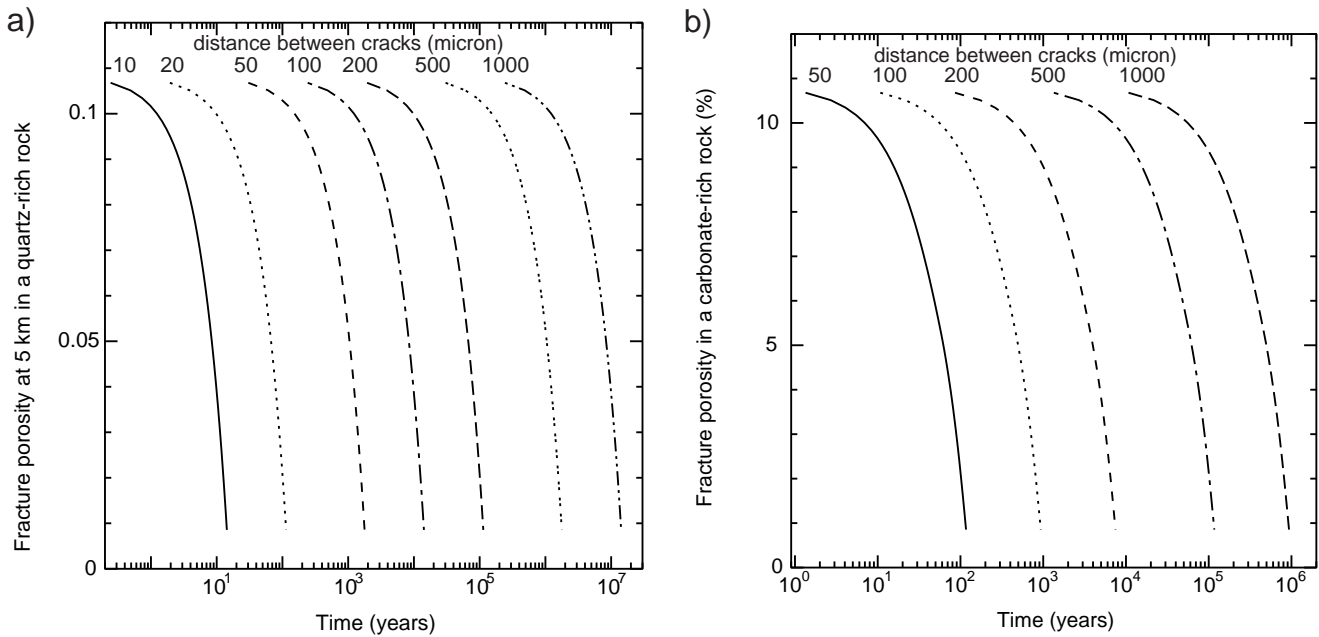


Fig. 7. (a) Size effect for simulations corresponding to the sealing of fractures of a quartz-rich rock at 5 km depth. The initial fracture porosity after an earthquake is the same in all cases. The rate of porosity decrease changes as the mean distance between the microcracks ( $L_{cs}$ ) varies from 10  $\mu\text{m}$  (a lot of small cracks), 20, 50, 100, 200, 500, to 1000  $\mu\text{m}$  (few larger cracks). The aperture of microcracks ( $L_v$ ) varies from 0.6, 1.2, 3, 6, 12, 30 to 60  $\mu\text{m}$ , respectively. The rate of crack sealing is much higher for a large number of small cracks than fewer larger ones. (b) Size effect for the sealing of fractures of a calcite-rich rock at 4 km depth. In this case also, the rate of sealing decreases when the mean distance between cracks increases (from 50, 100, 200, 500, to 1000  $\mu\text{m}$ ) and the crack thickness increases (3, 6, 12, 30, 60  $\mu\text{m}$ , respectively).

### 3.3. Sensitivity to various parameters

In these simulations, the least constrained parameters are the coefficient of diffusion along grain contacts or along the stylolites, the grain size that can vary locally in the fault; the crack width, and the mean distance between the veins (which imposes the area of dissolution under stress and thus the mean distance of diffusion along a trapped fluid). When these parameters vary, the time for fracture porosity closure is modified.

Decreasing the coefficient of diffusion of solutes from stylolites to open veins at a constant depth slows down pressure solution (Fig. 6). If the diffusion is as fast as in bulk water, the rate of pressure solution is two orders of magnitude higher. This parameter is, at this writing, the least constraint one in pressure solution models. It should strongly depend on the flatness of grain interfaces. We expect that new experiments in the coming years will help define more accurate values of this parameter and its dependence with temperature, and perhaps stress.

### 3.4. Effects of grain size and vein spacing

There is also a size effect, depending on the mean distance between veins (Fig. 7). A dense array of thin cracks will close much faster than a loose array of thicker cracks (Gratier et al., 1999). The larger the dis-

tance between stylolites and cracks, the slower is the transport from the dissolution site to the precipitation surface. Effect of the spacing between veins is given in Fig. 7. From 10  $\mu\text{m}$  to 1 mm, the strain rate decreases by six orders of magnitude. This is clearly the major effect and careful analysis of the main distance of mass transfer in natural deformation is required.

For distances comparable to those in Fig. 1 (100–200  $\mu\text{m}$  between stylolites), the sealing time of the fracture network in quartz-rich rocks at 4–6 km varies between 500 and 100 000 y depending on the value of the coefficient of diffusion. The lower value is close to the recurrence time of major earthquakes along active faults (Scholz, 1990).

The contributions of the different processes of pressure in the upper crust are summarized in Fig. 7 for the case of pure quartz or pure carbonate rocks. The rate of pressure solution in quartz rocks increases with depth both in the gouge and in the fractures with the difference that the gouge compaction is much faster than the fracture sealing because of the difference in the transport distance and the thickness of the dissolved and precipitated layers.

For carbonate rocks, the dependence of pressure solution with depth is more complex. The strain rate of pressure solution increases with depth, from 1 to 5 km. This rate decreases for greater depths because of a decrease of calcite solubility with temperature. The strain rate curves of carbonates rocks cross the curve

of quartz rocks at a temperature of 220–230°C, corresponding to depths of 7 km for a gradient of temperature of 30°/km (Fig. 8). Such calculations are in agreement with geological observations showing that calcite is mobile at shallow depths whereas quartz is more mobile at greater depths. The transition between these two fields is mainly controlled by temperature and by the chemistry of rocks and fluids.

#### 4. Discussion

Evans and Chester (1995) have observed that fluid-driven reactions and veining occurred during faulting, but are localized in a small region near the fault plane. For example, in the San Gabriel fault, geochemical data indicate that the system could have been opened to fluids for some time after an earthquake. As a fine-grained gouge compacts fast (several years according to our calculations), fluid could not circulate efficiently during a long period there, compared to open veins for which the kinetics of closing are much slower (several hundred to several million years). The distance to the fault over which the fluid can circulate should correspond to the area damaged by microfracturing around a fault during a seismic event.

In addition, geodetic observations of post-seismic deformation in the Northridge area show the presence of a creep deformation in the upper crust, associated with displacements on the surface over periods of several years (Donnellan and Lyzenga, 1998). These observations are in agreement with a deformation controlled by fluids and mechano-chemical processes in the upper crust. Our modeling indicates that such creep deformation can be caused by the two main processes of pressure solution: intergranular pressure solution, and dissolution along stylolite coupled to vein sealing.

Our calculations also suggest that permeability reduction around active faults in California should occur rapidly between 0 and 4 km because of calcite precipitation in open fractures. Below 7–8 km, the kinetics of quartz dissolution and precipitation are fast enough to allow quick vein sealing. As a consequence, there should exist a region in the crust characterized by slower porosity and permeability reduction, between 4 and 7 km. At this depth interval the decrease of calcite solubility slows down the process of vein sealing and the quartz kinetics are too slow to close fractures efficiently. Such calculations indicate that the local lithology is a crucial factor in controlling the rate of pressure solution-induced deformation in the crust.

The solubility crossover has significant implications for the distribution of pore pressure and its evolution during the seismic cycle. For example if calcite is mobilized at shallow depth, localized crack sealing is

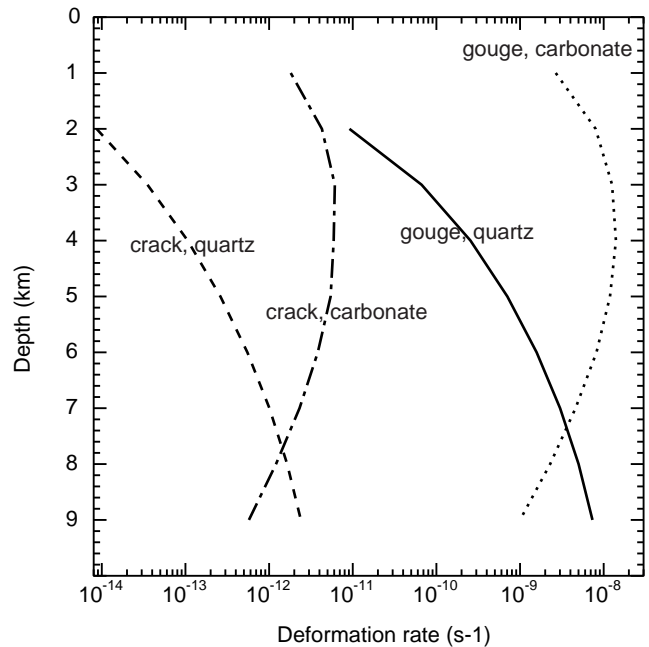


Fig. 8. Summary of the different processes of ductile deformation in an upper crust with carbonate rocks and quartz-rich rocks between 2 and 9 km. The two mechanisms of deformation presented here are compaction of a fine-grained gouge and sealing of open veins coupled with dissolution along stylolites. Gouge compaction is much faster than crack sealing and there is a clear control of the rate of deformation by the lithology. Such simulations are performed with textural and chemical variables that can be measured independently. Even if there can be a large uncertainty on some of the input parameters (rock texture, kinetics and thermodynamics data), it seems that the time scale of pressure solution creep can be relatively small and should play a role in the seismic cycle. Such calculations indicate also that there exists a transition depth in the crust. One passes from carbonate deformation at shallow depths to deformation accommodated by quartz-rich rocks at greater depths; the strain rates curves, crossing each other at a depth controlled by temperature, around 220°C in these simulations.

fast enough to induce a zone of low permeability promoting high pore pressure between 2 and 5 km depth.

Extrapolating this model to natural systems is clearly limited by the crucial effect of the geometry of the diffusion pathways. Geometric parameters such as the spacing between the cracks are not easy to estimate from natural observations. This is probably the main source of uncertainties in this approach. Careful studies must be performed in order to improve our knowledge of the three-dimensional geometry of such diffusion pathways.

Another uncertainty comes from the poor constraint on the relationship between stress and crack-seal kinetics. This needs a major experimental effort.

#### 5. Conclusions

Such calculations stress that viscous compaction of

the rocks inside a fault plays an important role during the seismic cycle and show that brittle and ductile deformation can interact in the upper crust (Gratier et al., 1999). Two time-scales emerge from our calculations based on natural observations: pervasive pressure solution at the grain scale in the gouge is much faster than pressure solution along stylolites and associated precipitation in veins. Following an earthquake, the permeability loss in the gouge, due to intergranular pressure solution, should be much faster than permeability variations due to fracture sealing. This suggests that open veins in the country rocks around the fault plane mainly control fluid circulation.

Fluids play a key role in the viscous relaxation occurring in the upper crust after an earthquake.

In the Northridge area, the post-seismic slip observed after the 1994 earthquake can reach several centimeters per year and is a witness of a 'soft upper crust'. Common explanations of this relaxation involve the flow of lower crustal material (Donnellan and Lyzenga, 1998). We suggest here that pressure solution may also be a mechanism of stress relaxation in the gouge and in the country rock surrounding the fault over periods of several days to hundreds of years after a major earthquake. We stress also that more experiments on pressure solution, and particularly on the rate of diffusion along grain boundaries, should help reducing the uncertainty concerning the time scales of this creep deformation.

### Acknowledgements

This project has been supported by the Norwegian Research Council through grant number 113354/420 to the Fluid–Rock Interactions. We would like to thank B. Parry and J. Hadzedej for helpful comments and J.P. Evans for his editorial help.

### References

- Applin, K.R., 1987. The diffusion of dissolved silica in dilute aqueous solution. *Geochimica and Cosmochimica Acta* 51, 2147–2151.
- Brace, W.F., Byerlee, J.D., 1966. Stick-slip as a mechanism for earthquakes. *Science* 153, 990–992.
- Byerlee, J.D., 1990. Friction, overpressure and fault normal compression. *Geophysical Research Letters* 17, 2109–2112.
- Chester, F.M., 1995. A rheologic model for wet crust applied to strike-slip faults. *Journal of Geophysical Research* 100, 13033–13044.
- Dewers, T., Ortoleva, P., 1990. A coupled reaction/transport/mechanical model for intergranular pressure solution stylolites, and differential compaction and cementation in clean sandstones. *Geochimica and Cosmochimica Acta* 54, 1609–1625.
- Donnellan, A., Lyzenga, D.A., 1998. GPS observations of fault after slip and upper crustal deformation following the Northridge earthquake. *Journal of Geophysical Research* 103, 21285–21297.
- Dove, P.M., 1994. The dissolution kinetics of quartz in sodium chloride solutions at 25°C to 300°C. *American Journal of Science* 294, 665–712.
- Evans, J.P., Chester, F.M., 1995. Fluid–rock interaction in faults of the San Andreas system: Inferences from San Gabriel fault rock geochemistry and microstructures. *Journal of Geophysical Research* 100, 13007–13020.
- Farver, J.R., Yund, R.Y., 1995. Interphase boundary diffusion of oxygen and potassium in K-feldspar/quartz aggregates. *Geochimica and Cosmochimica Acta* 59, 3697–3705.
- Farver, J.R., Yund, R.Y., 1999. Oxygen bulk diffusion measurements and TEM characterization of a natural ultramylonite for fluid transport in mica-bearing rocks. *Journal of Metamorphic Geology* 17, 669–684.
- Fisher, D.M., Brantley, S.L., Everett, M., Dzvonik, J., 1995. Cyclic fluid flow through a regionally extensive fracture network within the Kodiak accretionary prism. *Journal of Geophysical Research* 100, 12881–12894.
- Fisher, D.M., Brantley, S.L., 1992. Models of quartz overgrowth and vein formation; deformation and episodic fluid flow in an ancient subduction zone. *Journal of Geophysical Research* 97, 20043–20061.
- Fournier, R.O., 1996. Compressive and tensile failures at high fluid pressure where preexisting fractures have cohesive strength, with application to the San Andreas Fault. *Journal of Geophysical Research* 101, 25499–25509.
- Gibbs, J.W. 1877. On the equilibrium of heterogeneous substances. *Transactions of the Connecticut Academy* 3, 108–248 and 343–524.
- Gratier, J.P., Guiguet, R., 1986. Experimental pressure solution on quartz grains: the crucial effect of the nature of the fluid. *Journal of Structural Geology* 8, 845–856.
- Gratier, J.P., 1993. Experimental pressure solution of halite by an indenter technique. *Geophysical Research Letters* 20, 1647–1650.
- Gratier, J.P., Gamond, J.F., 1990. Transition between seismic and aseismic deformation in the upper crust. In: Knipe, R.J., Rutter, E.H. (Eds.), *Deformation, Mechanisms, Rheology and Tectonics*, Geological Society Special Publication, 54, pp. 461–473.
- Gratier, J.P., Chen, T., Hellmann, R., 1994. Pressure solution as a mechanism for crack sealing around faults, Proceedings of Workshop LXIII on the Mechanical involvement of fluids in faulting, 94–228. USGS open-file report, Menlo Park, CA, pp. 279–300.
- Gratier, J.P., Renard, F., Labaume, P., 1999. How pressure solution creep and fracturing process interact in the upper crust to make it behave in both a viscous and brittle manner. *Journal of Structural Geology* 21, 1189–1197.
- Gudmundsson, A., 1999. Fluid overpressure and stress drop in fault zones. *Geophysical Research Letters* 26, 115–118.
- Henderson, J.R., Maillot, B., 1997. The influence of fluid flow in fault zones on patterns of seismicity: a numerical investigation. *Journal of Geophysical Research* 102, 2915–2924.
- Hickman, S.H., Evans, B., 1991. Experimental pressure solution in halite—The effect of grain interphase boundary structure. *Journal of the Geological Society of London* 148, 549–560.
- Hickman, S., Sibson, R., Bruhn, R., 1995. Introduction to the special issue: mechanical involvement of fluid in faulting. *Journal of Geophysical Research* 100, 12831–12840.
- Janssen, C., Michel, W., Bau, M., Luders, V., Muhle, K., 1997. The North Anatolian Fault Zone and the role of fluids in seismogenic deformation. *Journal of Geology* 105, 387–403.
- Johnson, J.W., Oelkers, E.H., Helgeson, H.C., 1992. SUPCRT92—A software package for calculating the standard molal thermodynamic properties of minerals, gases, aqueous species, and reactions

- from 1 bar to 500 bar and 0°C to 1000°C. Computers and Geosciences 18, 899–947.
- Lachenbruch, A.H., 1980. Frictional heating, fluid pressure and the resistance to fault motion. Journal of Geophysical Research 85, 6097–6112.
- Lockner, D.A., Byerlee, J.D., 1995. An earthquake instability model based on faults containing high fluid-pressure compartments. Pure and Applied Geophysics 145, 717–745.
- Matthai, S.K., Fisher, G., 1996. Quantitative modeling of fault-fluid-discharge and fault-dilation-induced fluid-pressure variations in the seismogenic zone. Geology 24, 183–186.
- Marone, C., Raleigh, C.B., Scholz, C.H., 1990. Frictional behavior and constitutive modeling of simulated fault gouge. Journal of Geophysical Research 95, 8441–8452.
- Miller, S.A., Nur, A., Olgaard, D.L., 1996. Earthquakes as a coupled stress–high pore pressure dynamical system. Geophysical Research Letters 23, 197–200.
- Oelkers, E.H., Bjørkum, P.A., Murphy, W.M., 1996. A petrographic and computational investigation of quartz cementation and porosity reduction in North Sea sandstones. American Journal of Science 296, 420–452.
- Paterson, M.S., 1973. Nonhydrostatic thermodynamics and its geologic applications. Reviews of Geophysics and Space Physics 11, 355–389.
- Pili, E., et al. 1998. Isotope constraints on the involvement of fluids in the San Andreas Fault. Abstracts of Proceedings, AGU 1998 Spring Meeting.
- Plummer, L.N., Wigley, T.L.M., Parkhurst, D.L., 1978. The kinetics of calcite dissolution in CO<sub>2</sub>–water systems at 5° to 60°C and 0.0 to 1.0 atm CO<sub>2</sub>. American Journal of Science 278, 179–216.
- Plummer, L.N., Parkhurst, D.L., Wigley, T.L.M., 1979. Critical review of the kinetics of calcite dissolution and precipitation. In: Jenne, E.A. (Ed.), Chemical Modeling in aqueous systems, American Chemical Symposium Society Series, 93, pp. 537–573.
- Plummer, L.N., Busenberg, E., 1982. The solubilities of calcite, aragonite, and vaterite in CO<sub>2</sub>–H<sub>2</sub>O solutions between 0 and 90°C, and an evaluation of the aqueous model for the system CaCO<sub>3</sub>–CO<sub>2</sub>–H<sub>2</sub>O. Geochimica et Cosmochimica Acta 46, 1011–1040.
- Raj, R., Chung, C.K., 1981. Solution-precipitation creep in glass ceramics. Acta Metallurgica 29, 159–166.
- Raj, R., 1982. Creep in polycrystalline aggregates by matter transport through a liquid phase. Journal of Geophysical Research 87, 4731–4739.
- Renard, F., Ortoleva, P., 1997. Water films at grain–grain contacts: Debye–Hückel, osmotic model of stress, salinity and mineralogy dependence. Geochimica and Cosmochimica Acta 61, 1963–1970.
- Renard, F., Ortoleva, P., Gratier, J.P., 1997. Pressure solution in sandstones: Influence of clays and dependence on temperature and stress. Tectonophysics 280, 257–266.
- Renard, F., Park, A., Ortoleva, P., Gratier, J.P., 1999. An integrated model for transitional pressure solution in sandstones. Tectonophysics 312, 97–115.
- Rimstidt, J.D., Barnes, H.L., 1980. The kinetics of silica–water reactions. Geochimica and Cosmochimica Acta 44, 1683–1699.
- Rice, J.R., 1975. Continuum mechanics and thermodynamics of plasticity in relation to microscale deformation mechanisms. In: Argon, A.S. (Ed.), Constitutive Equations in Plasticity. MIT Press, Cambridge, Mass, pp. 23–79.
- Rice, J.R., 1992. Fault stress states, pore pressure distributions, and the weakness of the San Andreas Fault. In: Evans, B., Wong, T.-F. (Eds.), Fault Mechanics and Transport Properties in Rocks. Academic Press, London, pp. 475–503.
- Rudnicki, J.W., Chen, C.H., 1988. Stabilization of rapid frictional slip on a weakening fault by dilatant hardening. Journal of Geophysical Research 93, 4745–4757.
- Rutter, E., 1976. The kinetics of rock deformation by pressure solution. Philosophical Transactions of the Royal Society of London 283, 203–219.
- Segall, P., Rice, J.R., 1995. Dilatancy, compaction, and slip instability of a fluid-infiltrated fault. Journal of Geophysical Research 100, 22155–22171.
- Scholz, C.H., 1990. The Mechanics of Earthquakes and Faulting. Cambridge University Press, Cambridge.
- Shimizu, I., 1995. Kinetics of pressure solution creep in quartz: theoretical considerations. Tectonophysics 245, 121–134.
- Sleep, N.H., Blanpied, M.L., 1994. Ductile creep and compaction: A mechanism for transiently increasing fluid pressure in mostly sealed fault zones. Pure and Applied Geophysics 143, 9–40.
- Spiers, C.J., Schutjens, P.M., Brzesowsky, R.H., Peach, C.J., Liezenberg, J.L., Zwart, H.J., 1990. Experimental determination of constitutive parameters governing creep of rocksalt by pressure solution. In: Knipe, R.J., Rutter, E.H. (Eds.), Deformation Mechanisms, Rheology and Tectonics, Geological Society Special Publication, 54, pp. 215–227.
- Walderhaug, O., 1994. Precipitation rates for quartz cement in sandstones determined by fluid-inclusion microthermometry and temperature–history modeling. Journal of Sedimentary Research 64, 324–333.
- Weyl, P.K., 1959. Pressure solution and the force of crystallization: A phenomenological theory. Journal of Geophysical Research 69, 2001–2025.
- Yamashita, T., 1997. Mechanical effect of fluid migration on the complexity of seismicity. Journal Geophysical Research 102, 17797–17806.